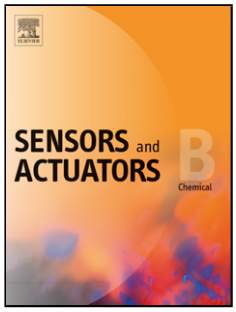

Title: Enhanced acetone sensing properties of titanium dioxide nanoparticles with a sub-ppm detection limit

Authors: S.T. Navale, Z. Yang, Chenshitao Liu, P. Cao, V.B. Patil, N.S. Ramgir, R.S. Mane, F.J. Stadler

PII: S0925-4005(17)31623-4
DOI: http://dx.doi.org/10.1016/j.snb.2017.08.186
Reference: SNB 23053

To appear in: *Sensors and Actuators B*

Received date: 4-5-2017
Revised date: 31-7-2017
Accepted date: 25-8-2017

Please cite this article as: S.T.Navale, Z.Yang, Chenshitao Liu, P.Cao, V.B.Patil, N.S.Ramgir, R.S.Mane, F.J.Stadler, Enhanced acetone sensing properties of titanium dioxide nanoparticles with a sub-ppm detection limit, Sensors and Actuators B: Chemicalhttp://dx.doi.org/10.1016/j.snb.2017.08.186

Enhanced acetone sensing properties of titanium dioxide nanoparticles with a sub-ppm detection limit

S. T. Navale[a,b], Z. Yang[a], Chenshitao Liu[a], P. Cao[a], V. B. Patil[c], N. S. Ramgir[d], R. S. Mane[e], F. J. Stadler[a*]

[a]College of Materials Science and Engineering, Shenzhen Key Laboratory of Polymer Science and Technology, Guangdong Research Center for Interfacial Engineering of Functional Materials, Nanshan District Key Laboratory for Biopolymers and Safety Evaluation, Shenzhen University, Shenzhen, 518060, PR China. (*E-mail: fjstadler@szu.edu.cn)

[b]Key Laboratory of Optoelectronic Devices and Systems of Ministry of Education and Guangdong Province, College of Optoelectronic Engineering, Shenzhen University, Shenzhen, 518060, PR China

[c]School of Physical Sciences, Solapur University, Solapur-413255, MS, India

[d]Technical Physics Division, Bhabha Atomic Research Centre, Trombay, Mumbai, 400085, India

[e]Center for Nanomaterials & Energy Devices, Swami Ramanand Teerth Marathwada University, Dnyanteerth, Vishnupuri, Nanded- 431606, India.

Graphical abstract

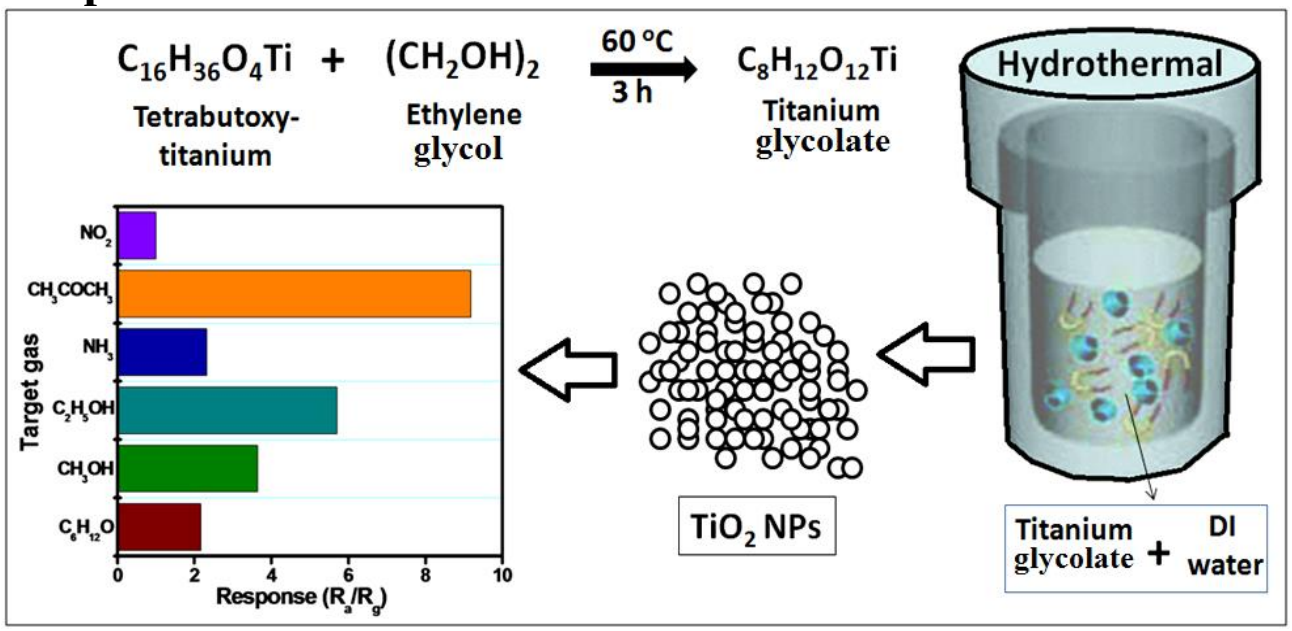

Highlights

- Simple hydrothermal synthesis strategy of TiO_2 NPs.
- Structural analysis confirms the formation of pure anatase phase of TiO_2 .
- TiO_2 sensor, composed of NPs, is highly sensitive and selective towards CH_3COCH_3 @270 °C.
- TiO_2 sensor demonstrates the enhanced response of 15.24 to 1000 ppm exposure of CH_3COCH_3 @270 °C along with rapid response and recovery times.
- TiO_2 sensor is able to detect as low as 500 ppb concentration of CH_3COCH_3.

Abstract

In the present study, a simple hydrothermal approach has been successfully applied for a large scale synthesis of anatase titanium dioxide nanoparticles (TiO_2 NPs) using titanium glycolate precursors and is utilized for the fabrication of low-cost high performance acetone (CH_3COCH_3) gas sensors after corroborating the crystallinity, phase-purity, and surface morphology investigations. Several randomly distributed TiO_2 aggregates, composed of NPs, are noticed from morphology analysis. Chemiresistive properties of as-fabricated TiO_2 sensors attempted towards host of oxidizing and reducing gases, reveal a superior selectivity to CH_3COCH_3 with a maximum response of 15.24 (1000 ppm) @270 °C compared to other target gases. One of the key features of as-fabricated TiO_2 sensor is the lowest detection limit of 500 ppb to CH_3COCH_3 with rapid response and recovery times, signifying commercial potential of the developed sensor materials. The effect of operating temperature along with various concentrations of CH_3COCH_3 on the gas sensing properties of TiO_2 sensor has thoroughly been investigated and reported. Finally, the interaction mechanism between the CH_3COCH_3 molecules

and the TiO_2 NPs sensor was elaborated in depth for a thorough understanding sensor performance experimentally and supposedly.

Keywords: Metal oxide; Hydrothermal synthesis; TiO_2 NPs; Chemiresistive properties; Acetone sensor

1. Introduction

In recent years, chemiresistive sensors based on semiconducting metal oxide nanostructures are a extensively investigated classes of gas sensors for developing efficient chemically stable and mechanically robust gas sensor devices for human safety and environmental monitoring applications due to their flexibility in production and low cost [1-13]. So far, the commercial traditional gas sensing devices have rapidly expanded, but they still failed to meet the demand of low-cost, high sensitivity, low detection limit, short response/recovery time, and lower temperature operation in combination. It is important to develop such kind of gas sensing materials, which detect the colorless and harmful gases at a very low concentration level as these gases are toxic in nature and have direct impact on human health and eco-system. Higher sensitivity and lower detection limit of a gas sensor material may sense a smaller quantity of leakaged gas, which eventually helps in avoiding serious accidents. Thus, to meet this demand, development of different materials using a variety of synthesis routes, *viz.* chemical and physical syntheses, are important to meet the challenges in the field of gas sensors. Till date, several semiconducting metal oxides such as tungsten oxide (WO_3) [1, 2, 4], tin dioxide (SnO_2) [3], zinc oxide (ZnO) [5, 6], cobalt oxide (Co_3O_4) [7], iron oxide (Fe_2O_3) [8, 9], titanium dioxide (TiO_2) [10, 11], nickel oxide (NiO) [12], and indium oxide (In_2O_3) [13] etc., have been reported as successful gas sensing materials for detecting a variety of toxic and inflammable gases with different detecting level capacities. Among known semiconducting metal oxides, nanostructured TiO_2 is one of the largely investigated materials for pigments in coating, gas sensor, self-cleaning glass, energy storage, photovoltaic, and photocatalysis applications because of its low-cost, high band gap energy, excellent chemical stability, and environmental friendliness [14-18]. A myriad of efforts have been undertaken successfully to synthesize TiO_2 nanostructures in different morphologies using hydrothermal [19], electrospinning [20], flame spray pyrolysis [21], sol-gel [22], anodization [23], matrix-assisted pulsed laser deposition [24], and screen printing [25] etc.,

followed the gas sensing application in literature. Amongst several known methods, hydrothermal synthesis is an easy and highly efficient chemical process used for obtaining nanostructures of metal oxides and chalcogenides at an ambient temperature. It is also well-known green approach because of its closed system conditions throughout the synthesis [26]. Moreover, hydrothermal process has quite a few advantages over other chemical methods in terms of economy, low-temperature, additives and catalyst-free, ability to scale up synthesis with high purity product, and environmental cordiality etc., [8, 19, 26]. Acetone, a colorless and clear liquid, is one of the general volatile organic compounds with the chemical formula CH_3COCH_3. Long-term inhalation of CH_3COCH_3 at high levels can cause fatigue, eye-irritation, headache, as well as nerve and kidney damage, as found by World Health Organization [27-29]. Furthermore, CH_3COCH_3, produced through hepatocytes by means of decarboxylation of excessacetyl-coenzyme A, is one of the commonly considered biomarkers for type-I as well as type-II diabetes [27, 28]. Thus, the development of low-cost high performance gas sensor systems, which can detect CH_3COCH_3 at low concentration levels, is crucial for the early diagnosis of diabetes in humans and process-control industry related applications.

In the present study, we have successfully synthesized anatase TiO_2 nanoparticles (NPs) using a titanium glycolate precursor through a simple hydrothermal route, which avoids the procedure of annealing treatment at elevated temperature, and which further were applied for the chemiresistive properties towards various target gases as well as operating temperatures. Initially, the as-synthesized TiO_2 NPs were characterized for confirming the structure and morphology by various means. Gas sensing properties demonstrate that the sensor based on TiO_2 NPs has a high sensitivity and selectivity towards acetone at an operating temperature of 270 °C. One of the key features of developed sensor is that it can detect acetone in parts per billion (ppb) levels with rapid response and recovery times.

2. Experimental

2.1 Materials

All chemicals [Tetrabutoxytitanium ($C_{16}H_{36}O_4Ti$), ethylene glycol [$(CH_2OH)_2$], acetone [$(CH_3)_2CO$], and CH_3CH_2OH] in the present study are of analytical grade and were used as received. Distilled water was used during all the experiment.

2.2 Synthesis of TiO_2 NPs

A low-temperature hydrothermal route was employed for the preparation of TiO_2 NPs using titanium glycolate as a source of Ti. Initially, the titanium glycolate precursor was produced using the procedure described in elsewhere with minor alterations [30]. In a typical procedure, 2.33 g of $C_{16}H_{36}O_4Ti$ was slowly added in 60 ml $(CH_2OH)_2$ and the desired mixture was magnetically stirred in a water bath @60 °C for 3 h. After the completion of reaction, the obtained clear solution was transferred into the $(CH_3)_2CO$ and distilled water mixture. The prepared suspension was then magnetically stirred for 2 h without any heat treatment. Subsequently, the obtained solid product was collected with the help of centrifugation and washed several times with distilled water and CH_3CH_2OH successively and dried @60 °C. Afterwards, the as-synthesized titanium glycolate precursor (0.5 gm) was dispersed in 30 ml of distilled water and the desired mixture was transferred to 50 ml capacity Teflon-lined autoclave. The hydrothermal reaction was carried out at 180 °C for 6 h and finally, synthesized TiO_2 product was collected by centrifugation followed by washing with distilled water and dried at 60 °C for 2 h. The schematic of formation of TiO_2 NPs using hydrothermal is shown in Fig. 1(a). Structural information of the as-synthesized TiO_2 product was investigated using X-ray diffraction spectroscopy (XRD, Model: Rigaku X-ray diffractometer with Cu-K_α source (λ=0.15418 nm)), Fourier infrared transform spectroscopy (FTIR, Model: Perkin-Elmer100 spectrophotometer), and X-ray photoelectron spectroscopy (XPS, Model: VG, Multilab 2000, Thermo VG, Scientific, UK). Morphology of TiO_2 was confirmed from digital images taken on scanning electron microscopy (SEM, Model: JEOL-6300F). Specific surface area and pore-size distribution of as-synthesized TiO_2 product were analyzed using Brunauer-Emmett-Teller (BET, Model: Belsorp II, BEL Japan Inc.) and Barrett–Joyner–Halenda (BJH) techniques, respectively.

2.3 Sensor fabrication and measurement

As-synthesized TiO_2 product was dispersed in distilled water in order to form a slurry/paste, which then was covered on a ceramic tube (4 mm length, external and internal diameter 1.2 mm and 0.8 mm, respectively), with the help of a paint brush, and thereafter used as sensing material. Both the ends of ceramic tube consist of two gold (Au) electrodes (0.5 mm wide each) for contacts, which are connected to platinum wires for signal collection (as shown in Fig. 5(b)). A Ni-Cr thermocouple was inserted inside the ceramic tube to control the operating temperature of sensor, which was managed by altering the heating current passed throughout the Ni-Cr coil. The gas sensing properties, in terms of change in electrical resistance, of as-

fabricated TiO_2 sensor were measured with the help of a static-test sensing system under laboratory conditions. The sensor was placed inside the airtight chamber (Volume: 20 L) and the certain amount of target gases inside the chamber was attained with the help of a micro-syringe. The recovery of sensors was achieved by allowing a fresh air inside the sensing chamber. The different kind of target gases such as CH_3COCH_3, ethanol (C_2H_5OH), methanol (CH_3OH), nitrogen dioxide (NO_2), ammonia (NH_3), and cyclohexanol ($C_6H_{12}O$) were tested. The response (S) of the sensor was calculated using following relation:

$$\text{Response (S)} = R_a/R_g \quad (1)$$

where R_a and R_g are the resistances of the sensor in presence of air and gas, correspondingly.

3. Results and discussion

3. 1 Structural elucidation and morphological evolution

A typical XRD pattern of as-synthesized TiO_2 NPs together with the Miller indices of the crystallographic planes corresponding to all the different diffraction peaks is shown in Fig. 1(b). The XRD pattern of TiO_2 reveals the diffraction peaks located at 2θ of 25.28°, 37.80°, 48.04°, 53.89°, 62.68°,68.76°, 70.30°, 75.10°, and 82.65°, belonging to (101), (004), (200), (105), (204), (116), (220), (215), and (224) Bragg's scattering planes, respectively. All observed diffraction peaks, without any additional impurity peaks, and their equivalent peak positions are analogous to the JCPDS Card #21-1272 of pure tetragonal anatase phase of TiO_2. The observed diffraction peaks are widened type, which is caused by the smaller size of the as-synthesized TiO_2. The average crystallite size in (101) direction is ≈14 nm, calculated from Scherrer relation ($D = 0.9\lambda/\beta.\cos\theta$, where D is the crystallite size, λ is the wavelength of X-ray, β is the full width at half maximum of (101) plane, and θ is the diffraction angle). The Raman spectrum of as-synthesized TiO_2 product is shown in Fig. 1(c), which obviously suggesting four active Raman peaks at 144, 397, 514, and 638 cm^{-1}. The highly intense peak observed at 144 cm^{-1} together with the peak located at 638 cm^{-1} is due to the E_g mode of anatase TiO_2. In addition to this, the peaks positioned at 397 and 514 cm^{-1} are due to B_{1g} and A_{1g} vibration modes, respectively. The peaks at 144 and 397 cm^{-1} confirm an involvement of the O-Ti-O bending vibration. However, the peaks at 514 and 638 cm^{-1} are of Ti-O stretching vibration. All observed Raman modes are entirely analogous to previously reported anatase TiO_2 [30, 31].

The wide range XPS spectrum of TiO_2 is shown in Fig. 2(a), suggesting the presence of Ti and O peaks. The core-level spectrum of Ti 2p, shown in Fig. 2(b), which demonstrates two

broad peaks belonging to Ti $2p_{3/2}$ and Ti $2p_{1/2}$ doublets situated at binding energies of 458.67 and 464.53 eV, respectively. The Ti $2p_{3/2}$ and Ti $2p_{1/2}$ doublet with the binding energy difference of 5.86 eV is the main characteristic of Ti^{+4} valance state of anatase TiO_2 in conjunction with octahedral co-ordination with O [32, 33]. The O1s core level spectrum of TiO_2, shown in Fig. 2(c), confirms major O1s peaks located at 530.1 and 531.93 eV. These peaks are assigned to the lattice oxygen (Ti-O-Ti) and hydroxyl (-OH) groups of TiO_2, continually, whereas the binding energy peak positioned at 533.57 eV is the characteristic of C=O [32-35]. Thus, the XPS study corroborates the formation of phase pure anatase TiO_2.

Surface morphology, playing an important role in gas sensing applications, of as-synthesized TiO_2 product was analyzed by SEM technique and presented in Fig. 3(a). The SEM surface image demonstrates that the closely bounded agglomerations of NPs. Random distribution of TiO_2 aggregates, composed of nanoparticles, with numerous pores stuck between them are clearly seen from the SEM micrograph. Such kind of surface morphology is preferred for gas sensing applications, since the circulation of target gas molecules is very fast through the porous structure compared to flat/dense surfaces, thereby, a higher performance is anticipated [36]. The EDX spectroscopy (Fig. 3(b)) was used to study the elemental composition present inside the synthesized TiO_2 product, which clearly suggesting that the synthesized product is composed of titanium (Ti) and oxygen (O). The information regarding the atomic percentages of Ti and O elements are given in the inset-table of Fig. 3(b). EDX mapping images of TiO_2 shown in Fig. 3(c) highlight the existence of O and Ti in the final product with appropriate proportions. Fig. 4(a) shows the nitrogen (N_2) adsorption/desorption isotherm of TiO_2 NPs obtained by hydrothermal method, suggesting a typical IV-type isotherm behavior along with H_3-type hysteresis loop [5, 7]. As-synthesized TiO_2 NPs exhibit a specific surface area of 25.2169 m^2/g and ~25 nm average pore-diameter (calculated using BJH pore size distribution curve, Fig. 4(b)), confirming an existence of the mesoporous character.

3. 2 Gas sensing properties

Gas sensing properties of the as-fabricated TiO_2 NPs sensor, whose on-field photograph is shown in Fig. 5(a), were studied towards NO_2, CH_3COCH_3, C_2H_5OH, CH_3OH, NH_3, and $C_6H_{12}O$ gases at different operating temperatures. The plot of response as a function of different target gases (500 ppm each), shown in Fig. 5(c), is suggesting that the TiO_2 NPs sensor displays maximum selectivity to CH_3COCH_3 gas in comparison to other test gases @270 °C. Therefore,

CH_3COCH_3 was considered as the selective target gas throughout the entire gas sensing study. The obtained response values for NO_2, CH_3COCH_3, C_2H_5OH, CH_3OH, NH_3, and $C_6H_{12}O$ gases are 1.2, 9.19, 5.71, 3.64, 2.32, and 2.17, respectively. The observed TiO_2 response value of 9.19 to 500 ppm CH_3COCH_3 is ~5 times higher than that of the fifth ranking $C_6H_{12}O$ gas. Selectivity coefficient (K) of CH_3COCH_3 over the other target gases was calculated using following relation [7]:

$$K=R_{CH3COCH3}/R_X \quad (2)$$

where $R_{CH3COCH3}$ and R_X are the responses of TiO_2 NPs sensor in presence of CH_3COCH_3 and other target gases (X). The calculated 'K' values for NO_2, C_2H_5OH, CH_3OH, NH_3, and $C_6H_{12}O$ are 7.65, 1.59, 2.52, 3.96, and 4.23, respectively. Higher 'K' value suggested that the as-fabricated sensor has a superior ability to discriminate the target gas (here CH_3COCH_3) between the mixture of gases. It is well-known that the operating temperature significantly influences the gas sensing properties of sensors based on semiconducting metal oxides [36-40]. Thus, the effect of operating temperature on the gas sensing performances of TiO_2 sensors was thoroughly studied and obtained results are displayed in Fig. 5(d). For the response study of TiO_2 NPs sensor, with respect to operating temperature, a fixed 500 ppm concentration of CH_3COCH_3 was used. The TiO_2 sensor starts responding to CH_3COCH_3 at the operating temperature of 250 °C and attains the maximum response value at 270 °C. The response value of TiO_2 sensors above 270 °C is decreased with increasing temperature. A maximum response value of 9.19 at 270 °C upon 500 ppm exposure of CH_3COCH_3 is obtained; as a result 270 °C was used as an optimized sensing temperature for TiO_2 NPs sensor in further gas sensing studies. TiO_2 is a well known catalyst for CH_3COCH_3. At its surface acetone undergoes oxidation to CO_2 and H_2O in the presence of adsorbed oxygen [41]. The adsorbed oxygen molecules help to improve the response while the moisture present on the sensor surface hinders the CH_3COCH_3 oxidation. Gas sensing response, being a surface phenomenon, strongly depends on the adsorption and desorption kinetics and usually exhibits volcanic shape temperature dependence (see Fig. 5(d)). Here, the sensor response first increases with temperature, attains a maximum and then decreases with further rise in temperature. This behavior is attributed to the temperature dependence of adsorption and desorption rates and can be explained by considering the surface reactions and gas diffusion kinetics [42, 43]. Initially, with temperature, the adsorption increases while at higher temperatures desorption of gases or molecular oxygen from the sensor surface is more

favorable. Besides, at higher temperatures the low utilization rate of the sensing material is owing to low gas adsorption ability of the gas molecule causes poor response [44]. At equilibrium, a maximum response towards CH_3COCH_3 is owing to suitable activation energy and enhanced reaction rate [44, 45]. At this temperature, the high selectivity is attributed to the higher adsorption activities of the TiO_2 surfaces for CH_3COCH_3 as compared to that of other investigated gases [46, 47]. Thus, based on the selectivity and temperature dependent response study it is concluded that the TiO_2 NPs sensor of anatase phase is highly sensitive and selective to CH_3COCH_3 gas in comparison to other target gases @270 °C. Thereafter, the effect of CH_3COCH_3 concentration (0.5-500 ppm) on TiO_2 sensors was studied thoroughly @270 °C and reported herein.

The dynamic resistance plot of TiO_2 NPs sensor upon 0.5-500 ppm levels exposure of CH_3COCH_3 at the operating temperature of 270 °C is shown in Fig. 6(a). One of the key features of fabricated TiO_2 sensor is the lowest detection limit of CH_3COCH_3. TiO_2 NPs sensor is capable to detect as low as 0.5 ppm (500 ppb) of CH_3COCH_3 with response of 1.18. The variation of TiO_2 response as a function of CH_3COCH_3 concentration is shown in Fig. 6(b), demonstrating the increase in response value with CH_3COCH_3 concentration. A maximum 15.24 response of 15.24 is evidenced to 1000 ppm exposure of CH_3COCH_3. Low response at lower concentrations of CH_3COCH_3 attributes to the lower surface coverage of CH_3COCH_3 gas molecules as a result of lower surface interactions, which limits the sensor response. Conversely, a higher concentration of CH_3COCH_3 covers increasingly surface of TiO_2, which eventually enhances the surface interactions, consequently, increases the response value.

The reversibility study of as-fabricated TiO_2 NPs sensor upon random concentration of CH_3COCH_3 is shown in Fig. 6(c), suggesting the sensor shows higher reversibility and reproducibility towards CH_3COCH_3 with identical sensor response values and response kinetics. The observed response values to 10, 100, 50, and 200 ppm CH_3COCH_3 are 1.67, 4.25, 3.19, and 6, respectively. From Fig. 6(c) it is clear that, the as-fabricated sensor exhibits an excellent reversibility upon successive low and high levels exposure of CH_3COCH_3. The response and recovery times, considered as key parameters of the chemiresistive-type of sensors, were measured and defined as the time taken by sensor to attain 90% of its maximum resistance change in case of adsorption and desorption, correspondingly [48]. Ideal gas sensors supposed to have a rapid response and recovery times. The response-recovery plot of TiO_2 sensor upon 500

ppm exposure of CH_3COCH_3 @270 °C is shown in Fig. 7(a), demonstrating a rapid response time of 10 s and recovery time of 9 s. Precise reproducible feature along with nearly square shaped response have clearly been evidenced from the response-recovery plot (Fig. 7(a)) [49]. It is observed that, initially, the TiO_2 sensor has responded rapidly to CH_3COCH_3 and quickly has attained a nearly stable state. Afterwards, the sensor is reached to its baseline level, when exposed to fresh air. From the viewpoint of practical application of sensors, not only higher responses and rapid response-recovery times but also reproducibility and stability in response are considered as essential parameters too. Hence, reproducibility, and stability of TiO_2 NPs sensor to CH_3COCH_3 were studied systematically and reported herein. The response repeatability study towards consecutive five cycles of 500 ppm CH_3COCH_3@270 °C was carried out and the obtained results are displayed in Fig. 7(b). Almost the same response value of ~9.19 is achieved upon successive exposure of CH_3COCH_3, demonstrating the excellent reproducibility in response of TiO_2 sensor toward CH_3COCH_3. The plot of stability study of TiO_2 sensor, for the period of 10 days, towards fixed a 500 ppm concentration of CH_3COCH_3 @270 °C is shown in Fig. 7(c). The stability study demonstrates that the TiO_2 NPs sensor had retained its response value superbly. The observed gas sensing properties such as response, selectivity, response-recovery times, reproducibility, and stability of the TiO_2 sensor makes it suitable candidate for selective and sub-ppm detection of CH_3COCH_3 in variety of applications. We have compared the CH_3COCH_3 sensing performance of hydrothermally grown TiO_2 NPs with those of reports available in literature for TiO_2 simply and the comparison is tabulated in table 1. From the table, it can be clearly noticed that the as-fabricated TiO_2 NPs sensor is demonstrating excellent sensing properties, in terms of lowest detection limit, rapid response and recovery times, and lower operating temperature, than that of results quoted in literature.

3. 3 Gas sensing mechanism

It is well-known that the gas sensing mechanism of semiconducting metal oxides depends upon the change in their electrical resistance signatures, which primarily is caused by means of the adsorption/desorption of target gas molecules on the top of sensor surface, upon the interaction of different target gases. As the TiO_2 sensor is exposed to fresh air, oxygen molecules from air adsorb on the TiO_2 surfaces, by capturing electrons form the conduction band of TiO_2 resulting in the formation of an electron depletion layer (as shown in Fig. 8) leading to the higher resistance, which forms the adsorbed oxygen species (such as O^-, O_2^-, and O^{2-}). Adsorbed

oxygen has temperature dependent character [5]. It has O_2^- nature below 100 °C, O^- in between 100-300 °C, and O^{2-} above 300 °C. In the present case, the sensor temperature is 270 °C thus, the O^- species are dominants. The adsorption on the sensor surface takes place as per following reactions (wherein *'a'* stands for air, *'ad'* stands for adsorption, and *'g'* stands for gas):

$$O_{2\,(a)} \longrightarrow O_{2\,(ad)} \quad (3)$$

$$O_{2\,(ad)} + e^- \longrightarrow O_{2\,(ad)}^- \quad (4)$$

$$O_{2\,(ad)}^- + e^- \longrightarrow 2O_{(ad)}^- \quad (5)$$

Herein, TiO_2 is n-type semiconductor with electrons (e^-) as majority carriers. The thermal activation barrier between adsorbed acetone and oxygen to form the acetone-oxygen complex is 10 kJ/mol [45]. The first principle calculations have revealed that the adsorption energy for acetone on TiO_2 surface is negative indicating the process to be exothermic and spontaneous [46]. Hence, when reducing CH_3COCH_3 gas molecules come in contact with the TiO_2 sensor, the previously adsorbed oxygen species readily interact with the organic gas molecules by releasing the trapped e^- back to the conduction band of TiO_2. Thereby, the conductivity of TiO_2 increases due to the e^- donating nature of CH_3COCH_3 and consequently, the resistance decreases. Decrease in resistance of TiO_2 leads to the reduction in the size of electron depletion layer as shown in the schematic of Fig. 8. Thus, it is prevalent that the adsorbed oxygen molecules on the sensor surface play a dominating role in the governing sensing mechanism. The possible reaction mechanism is as follows [20, 49]:

$$CH_3COCH_{3\,(g)} \longrightarrow CH_3COCH_{3\,(ad)} \quad (6)$$

$$CH_3COCH_{3\,(ad)} + 4\,O_{(ad)}^- \longrightarrow 3CO_{2(g)} + 3H_2O + 4e^- \quad (7)$$

4. Conclusions

A simple and rapid hydrothermal chemical strategy has been successfully applied for the synthesis of anatase TiO_2 NPs and their chemiresistive activity has been envisaged towards various target gases. Gas sensing results demonstrate that the TiO_2 NPs-based sensor has high selectivity to CH_3COCH_3 and capable to detect its concentration up to ppb level limit at an operating temperature of 270 °C. Our gas sensing results suggest that the as-fabricated TiO_2 sensors is a fascinating candidate for the development of low-cost high performance CH_3COCH_3-based sensors, in view of its excellent selectivity, lower detection limit, rapid

response/recovery times, and outstanding dynamic properties along with the high response in stability.

Acknowledgements

The authors would like to thank the National Science Foundation of China (21574086), Nanshan District Key Lab for Biopolymers and Safety Evaluation (No. KC2014ZDZJ0001A), Shenzhen Sci & Tech Research grant (ZDSYS201507141105130), and Shenzhen City Science and Technology Plan Project (JCYJ20140509172719311) for financial support.

References

[1] C. Wang, R. Z. Sun, X. Li, Y. F. Sun, P. Sun, F. M. Liu, G.Y. Lu, Hierarchical flower-like WO_3 nanostructures and their gas sensing properties, Sens. Actua. B, 204 (2014) 224–230.

[2] D. L. Chen, L. F. Ge, L. Yin, H. Y. Shi, D. W. Yang, J. Yang, R. Zhang, G. S. Shao, Solvent-regulated solvothermal synthesis and morphology-dependent gas-sensing performance of low-dimensional tungsten oxide nanocrystals, Sens. Actua. B, 205 (2014) 391–400.

[3] G. D. Khuspe, R. D. Sakhare, S. T. Navale, M. A. Chougule, Y. D. Kolekar, R. N. Mulik, R. C. Pawar, C. S. Lee, V. B. Patil, Nanostructured SnO_2 thin films for NO_2 gas sensing applications, Cera. Inter., 39 (2013) 8673–8679.

[4] D. L. Chen, L. Yin, L. F. Ge, B. B. Fan, R. Zhang, J. Sun, G.S. Shao, Low-temperature and highly selective NO-sensing performance of WO_3 nanoplates decorated with silver nanoparticles, Sens. Actua. B, 185 (2013)445–455.

[5] S. T. Navale, V. V. Jadhav, K. K. Tehare, R.U.R. Sagar, C. S. Biswas, M. Galluzzi, W. Liang, V. B. Patil , R. S. Mane, F. J. Stadler, Solid-state synthesis strategy of ZnO nanoparticles for the rapid detection of hazardous Cl_2, Sens. Actua. B, 238 (2017) 1102–1110.

[6] H. N. Hieu, N. M. Vuong, H. Jung, D. M. Jang, D. Kim, H. Kim, S. K. Hong, Optimization of a zinc oxide urchin-like structure for high-performance gas sensing, J. Mater. Chem., 22 (2012) 1127–1134.

[7] S. T. Navale, C. Liu, P. S. Gaikar, V. B. Patil, R.U.R. Sagar, B. Du, R.S. Mane, F. J. Stadler, Solution-processed rapid synthesis strategy of Co_3O_4 for the sensitive and selective detection of H_2S, Sens. Actua. B, 245 (2017) 524–532.

[8] X. Hu, J. C. Yu, J. Gong, Q. Li, G. Li, α-Fe_2O_3nanorings prepared by a microwave-assisted hydrothermal process and their sensing properties, Adv. Mater., 19 (2007) 2324–2329.

[9] S. T. Navale, D. K. Bandgar, S. R. Nalage, G. D. Khuspe, M. A. Chougule, Y. D. Kolekar, S. Sen, V. B. Patil, Synthesis of Fe_2O_3 nanoparticles for nitrogen dioxide gas sensing applications, Cera. Inter., 39 (2013) 6453–6460.

[10] L. P. Liu, X. G. Li, P. K. Dutta, J. Wang, Room temperature impedance spectroscopy-based sensing of formaldehyde with porous TiO_2 under UV illumination, Sens. Actua., B, 185 (2013) 1–9.

[11] H.-Y. Yang, X.-L. Cheng, X.-F. Zhang, Z.-K. Zheng, X.-F. Tang, Y.-M. Xu, S. Gao,H. Zhao, L.-H. Huo, A novel sensor for fast detection of triethylamine based on rutile TiO_2 nanorod arrays, Sens. Actua. B, 205 (2014) 322–328.

[12] B. Liu, H. Q. Yang, H. Zhao, L. J. An, L. H. Zhang, R.Y. Shi, L. Wang, L. Bao, Y. Chen, Synthesis and enhanced gas-sensing properties of untralong NiO nanowires assembled with NiO nanocrystals, Sens. Actua. B, 156(2011) 251–262.

[13] X. X. Xu, X. D. Mei, P. L. Zhao, P. Sun, Y. F. Sun, X. L. Hu, G. Y. Lu, One-step synthesis and gas sensing characteristics of urchin-like In_2O_3, Sens. Actua. B, 186 (2013) 61–66.

[14] C. Garzella, E. Comini, E. Tempesti, C. Frigeri, G. Sberveglieri, TiO_2 thin films by a novel sol–gel processing for gas sensing applications, Sens. Actua. B, (2000) 189–196.

[15] M. Ferroni, M. C. Carotta, V. Guidi, G. Martinelli, F. Ronconi, M. Sacerdoti, E. Traversa, Preparation and characterization of nanosized titania sensing film, Sens. Actua. B, 77 (2001) 163–166.

[16] S. T. Navale, K. K. Tehare, S. F. Shaikh, V. B. Patil, B. N. Pawar, M. Naushad, F. J. Stadler, R. S. Mane, Hexamethylenetetramine-mediated TiO_2 films: Facile chemical synthesis strategy and their use in nitrogen dioxide detection, Mat. Lett., 173 (2016) 9–12.

[17] S. Ameen, M. S. Akhtar, H. K. Seo, H. S. Shin, Ti thin film towards the growth of crystalline-TiO_2 nanostructures: stepped light-induced transient measurements of photocurrent and photovoltage in dye sensitized solar cell, Cryst. Eng. Comm., 16 (2014) 3020–3028.

[18] K. Zakrzewska, Mixed oxides as gas sensors, Thin Solid Films, 391 (2001) 229-238.

[19] L. Huang, T. M. Liu, H. J. Zhang, W. W. Guo, W. Zeng, Hydrothermal Synthesis of Different TiO_2 Nanostructures: Structure, Growth and Gas Sensor Properties. J. Mater. Sci.: Mater. Electron., 23 (2012) 2024−2029.

[20] H. Bian, S. Ma, A. Sun, X. Xu, G. Yang, J. Gao, Z. Zhang, H. Zhu, Characterization and acetone gas sensing properties of electrospun TiO_2 nanorods, Superlat. Microstru., 81 (2015) 107–113.

[21] S. Phanichphant , C. Liewhiran, K. Wetchakun, A. Wisitsoraat, A. Tuantranont, Flame-made Nb-doped TiO_2 ethanol and acetone sensors, Sensors, 11 (2011) 472-484.

[22] D. M. Tobaldi, S. G. Leonardi, R. C. Pullar, M. P. Seabra, G. Neri J. A. Labrinch, Sensing properties and photochromism of Ag–TiO_2 nano-heterostructures, J. Mater. Chem. A, 4 (2016) 9600-9613.

[23] P. Bhattacharyya, B. Bhowmik and H. J. Fecht, Operating temperature, repeatability, and selectivity of TiO_2 nanotube-based acetone sensor: Influence of Pd and Ni nanoparticle modifications, IEEE Trans. Mater. Real., 15 (3) (2015) 376-383.

[24] R. Rella, J. Spadavecchia, M. G. Manera, S. Capone, A. Taurino, M. Martino, A. P. Caricato, T. Tunno, Acetone and ethanol solid-state gas sensors based on TiO_2 nanoparticles thin film deposited by matrix assisted pulsed laser evaporation, Sens. Actua. B, 127 (2007) 426–431.

[25] L. L. Deng, C. X. Zhao, Y. Ma, S. S. Chen, G. Xu, Low cost acetone sensors with selectivity over water vapor based on screen printed TiO_2 nanoparticles, Anal. Methods, 5 (2013) 3709–3713.

[26] S. Komarneni, Y. D. Noh, J. Y. Kim, S. H. Kim, H. Katsuki, Solvothermal/Hydrothermal synthesis of metal oxides and metal powders with and without Microwaves, Z. Naturforsch., 65 (2010) 1033-1037.

[27] D. J. Reisman, International programme on chemical safety ed. Acetone, World Health Organization, Geneva, 1998.

[28] T. Xiao, X. Y. Wang, Z.H. Zhao, L. Li, L. Zhang, H. C. Yao, J. S. Wang, Z. J. Li, Highly sensitive and selective acetone sensor based on C-doped WO_3 for potential diagnosis of diabetes mellitus, Sens. Actua. B, 199 (2014) 210-219.

[29] K. W. Kao, M. C. Hsu, Y. H. Chang, S. Gwo, J. A. Yeh A sub-ppm acetone gas sensor for diabetes detection using 10 nm thick ultrathin InN FETs, Sensors, 12 (2012) 7157-7168.

[30] G. Cheng, M. S. Akhtar, O. Yang, F. J. Stadler, Novel Preparation of Anatase TiO_2@Reduced graphene oxide hybrids for high-performance dye-sensitized solar cells, ACS Appl. Mater. Interfaces, 5 (2013) 6635−6642.

[31] T. Ohsaka, F. Izumi, Y. Fujiki, Raman Spectrum of Anatase, TiO_2, J. Raman Spectro., 7 (6) (1978) 321-324.

[32] P. B. Patil, S. S. Mali, V. V. Kondalkar, N. B. Pawar, K. V. Khot, C. K. Hong, P. S. Patil, P. N. Bhosale, Single step hydrothermal synthesis of hierarchical TiO_2 microflowers with radially assembled nanorods for enhanced photovoltaic performance, RSC Adv., 4 (2014) 47278–47286.

[33] E. McCaerty, J. P. Wightman, Determination of the concentration of surface hydroxyl groups on metal oxide films by quantitative XPS method, Surf. Interface. Anal., 26 (1998) 549.

[34] V. V. Kondalkar, S. S. Mali, N. B. Pawar, R. M. Mane, S. Choudhury, C. K. Hong, P.S. Patil, S. R. Patil, P.N. Bhosale, J. H. Kim, Microwave-assisted rapid synthesis of highly porous TiO_2 thin films with nanocrystalline framework for efficient photoelectrochemical conversion, Electro. Acta, 143 (2014) 89–97.

[35] J. Li, H.C. Zeng, Preparation of Monodisperse Au/TiO_2 Nanocatalysts via Self assembly, Chem. Mater. 18 (2006) 4270.

[36] S. T. Navale, A. T. Mane, M. A. Chougule, N. M. Shinde, J. H. Kim, V. B. Patil, Highly selective and sensitive CdS thin film sensors for detection of NO_2 gas, RSC Adv., 4 (2014) 44547–44554.

[37] S. T. Navale, D. K. Bandgar, M. A. Chougule, V. B. Patil, Facile method of preparation of PbS films for NO_2 detection, RSC Adv., 5 (2015) 6518–6527.

[38] S. T. Navale, G. D. Khuspe, M. A. Chougule, V. B. Patil, Polypyrrole, α-Fe_2O_3 and their hybrid nanocomposite sensor: An impedance spectroscopy study, Org. Electro., 15 (2014) 2159–2167.

[39] X. Zhou, W. Feng, C. Wang, X. Hu, X. Li, P. Sun, K. Shimanoe, N. Yamazoe, G. Lu, Porous ZnO/$ZnCo_2O_4$ hollow spheres: synthesis, characterization, and applications in gas sensing, J. Mater. Chem. A, 2 (2014) 17683.

[40] A. T. Mane, S. T. Navale, S. Sen, D. K. Aswal, S. K. Gupta , V. B. Patil, Nitrogen dioxide (NO_2) sensing performance of p-polypyrrole/ n-tungsten oxide hybrid nanocomposites at room temperature, Org. Electro., 16 (2015) 195–204.

[41] M. El-Maazawi, A. N. Finken, A. B. Nair, V. H. Grassian, Adsorption and Photocatalytic Oxidation of Acetone on TiO_2: An in Situ Transmission FT-IR Study, J. Catalysis, 191(2000)138–146.

[42] G. Sakai, N. Matsunaga, K. Shimanoe, N. Yamazoe, Theory of Gas-diffusion Controlled Sensitivity for Thin Film Semiconductor Gas Sensor, Sens. Actua. B, 80 (2001) 125−131.

[43] M. A. Henderson, Photooxidation of Acetone on TiO2 (110): Conversion to Acetate via Methyl Radical Ejection, J. Phys. Chem. B, 109 (2005) 12062-12070.

[44] N. Chen, Y. Li, D. Deng, X. Liu, X. Xing, X. Xiao, Y. Wang, Acetone sensing performances based on nanoporous TiO_2 synthesized by a facile hydrothermal method, Sens. Actua. B, 238 (2017) 491-500.

[45] C. A. Betty, S. Choudhury, Charge carrier transport in nanocrystalline SnO_2 thin film sensor and temperature dependence of toxic gas sensitivity, Sens. Actua. B, 237 (2016) 787-794.

[46] Y. Yang, Y. Liang, G. Wang, L. Liu, C. Yuan, T. Yu, Q. Li, F. Zeng, G. Gu, Enhanced gas-sensing properties of the hierarchical TiO_2 hollow microspheres with exposed high-energy {001} crystal facets, ACS Appl. Mater. Inter., 7 (2015) 24902−24908.

[47] N. Bahadur, K. Jain, R. Pasricha, B. Govind, S. Chand, Selective gas sensing response from different loading of Ag in sol-gel processed mesoporous titania powders, Sens. Actua. B, 159 (2011) 112–120.

[48] C. Wang, J. Liu, Q. Yang, P. Sun, Y. Gao, F. Liu, J. Zheng, G. Lu, Ultrasensitive and low detection limit of acetone gas sensor based on W-doped NiO hierarchical nanostructure, Sens. Actua. B, 220 (2015) 59–67.

[49] X. Zhou, B. Wang, H. Sun, C. Wang, P. Sun, X. Li, X. Hu, G. Lu, Template-free synthesis of hierarchical $ZnFe_2O_4$ yolk–shell microspheres for high-sensitivity acetone sensors, Nanoscale, 8 (2016) 5446-5453.

[50] B. Bhowmik, V. Manjuladevi, R. Gupta, P. Bhattacharyya, Highly selective low-temperature acetone sensor based on hierarchical 3-D TiO_2 nanoflowers, IEEE Sens. J., 16 (10) (2016) 3488-3495.

[51] A. P. Caricato, S. Capone, G. Ciccarella, M. Martino, R. Rella, F. Romano, J. Spadavecchi, A. Taurino, T. Tunno, D. Valerini, TiO_2 nanoparticle thin film deposition by matrix assisted pulsed laser evaporation for sensing applications, Appl. Surf. Sci., 253 (2007) 7937–7941.

[52] X. Cheng, Y. Xu, S. Gao, H. Zhao, L. Huo, Ag nanoparticles modified TiO_2 spherical heterostructures with enhanced gas-sensing performance, Sens. Actua. B, 155 (2) (2011) 716–721.

Bibliography

S. T. Navale received his M.Sc. (2012) and Ph. D. (2015) in Physics from the School of Physical Sciences, Solapur University, Solapur, India. Currently he is actively involved in the synthesis of metal oxides and conducting polymer/graphene oxide based nanocomposites for gas sensor and energy storage applications.

Z. Yang is a MS student at College of Materials Science and Engineering, Shenzhen University, Shenzhen, China. Currently he is actively involved in the synthesis of metal oxide based nanocomposites for the application of high performance gas sensors.

C. Liu is a MS student at College of Materials Science and Engineering, Shenzhen University, Shenzhen, China. Currently he is actively involved in the synthesis of metal oxides by variety of synthesis routes for the application of high performance gas sensors.

P. Cao is an associate professor at the College of Materials Science and Engineering, Shenzhen University, Shenzhen, China. He received his BS in Infrared Optics from the Changchun Institute of Optics and Fine Mechanics (1995) and Ph.D. in Condensed Matter Physics from Jilin University (2001). Dr. Cao's research interests include the growth of nanoscale functional materials and their applications in gas sensor and field emission properties.

V. B. Patil is a professor School of Physical Sciences, Solapur University, Solapur, MS, India. He has authored and co-authored more than 80 publications. His research interests include gas sensors, DSSCs, and supercapacitors.

N. S. Ramgir completed his Ph.D. (Physics) in 2006 from National Chemical Lab-oratory, Pune, India. After completing his Humboldt fellowship at Nanotechnology Group, University of Freiburg, Germany, he joined Bhabha Atomic Research Centre as Scientific Officer. His current research work is focused on applications of semi-conducting oxides based thin films and nanostructures for gas sensors.

R. S. Mane is a professor and visiting professor at School of Physical Sciences, SRTM University, Nanded and at KSU, Saudi Arabia, respectively. His research interests include solid and liquid state DSSCs, supercapacitors, and gas sensors.

F. J. Stadler is a distinguished professor at College of Materials Science and Engineering, Shenzhen University, Shenzhen, China. He has authored and co-authored more than 100 publications. His research interests include soft matter physics, rheology, DSSCs, and chemical sensors.

Figure captions

Fig. 1(a) Synthesis scheme of TiO_2 NPs, (b) XRD, and (c) Raman spectrums of as-synthesized anatase TiO_2.

Fig. 2(a) Wide range, (b) Ti 2p, and (c) O1s XPS spectrums of TiO_2.

Fig. 3(a) SEM and (b) EDX spectrum, and (c, d, e) EDX elemental mapping images of TiO_2.

Fig. 4(a) N_2 adsorption-desorption isotherm, and (b) BJH pore size distribution plot of as-synthesized TiO_2.

Fig. 5(a) Photograph of as-fabricated TiO_2 sensor, (b) Schematic view of fabrication of sensor, (c) Selectivity study of TiO_2 sensor towards various target gases at fixed 500 ppm concentration @270 °C, and (d) Temperature dependent CH_3COCH_3 response values of TiO_2 sensor.

Fig. 6(a) Dynamic resistance plot of TiO_2 sensor towards various concentrations of CH_3COCH_3 @270 °C, (b) Plot of response as a function of CH_3COCH_3 concentrations @270 °C, (c) Reversibility study of TiO_2 sensor upon random concentration of CH_3COCH_3 @270 °C.

Fig. 7(a) Response-recovery plot of TiO_2 sensor upon 500 ppm exposure of CH_3COCH_3, (b) Reproducibility study of TiO_2 sensor towards successive exposure of CH_3COCH_3, and (c) Stability study of TiO_2 sensor upon fixed 500 ppm exposure of CH_3COCH_3 @270 °C.

Fig. 8 Schematic of gas sensing mechanism of TiO_2 sensor in presence of air and CH_3COCH_3 atmosphere, respectively.

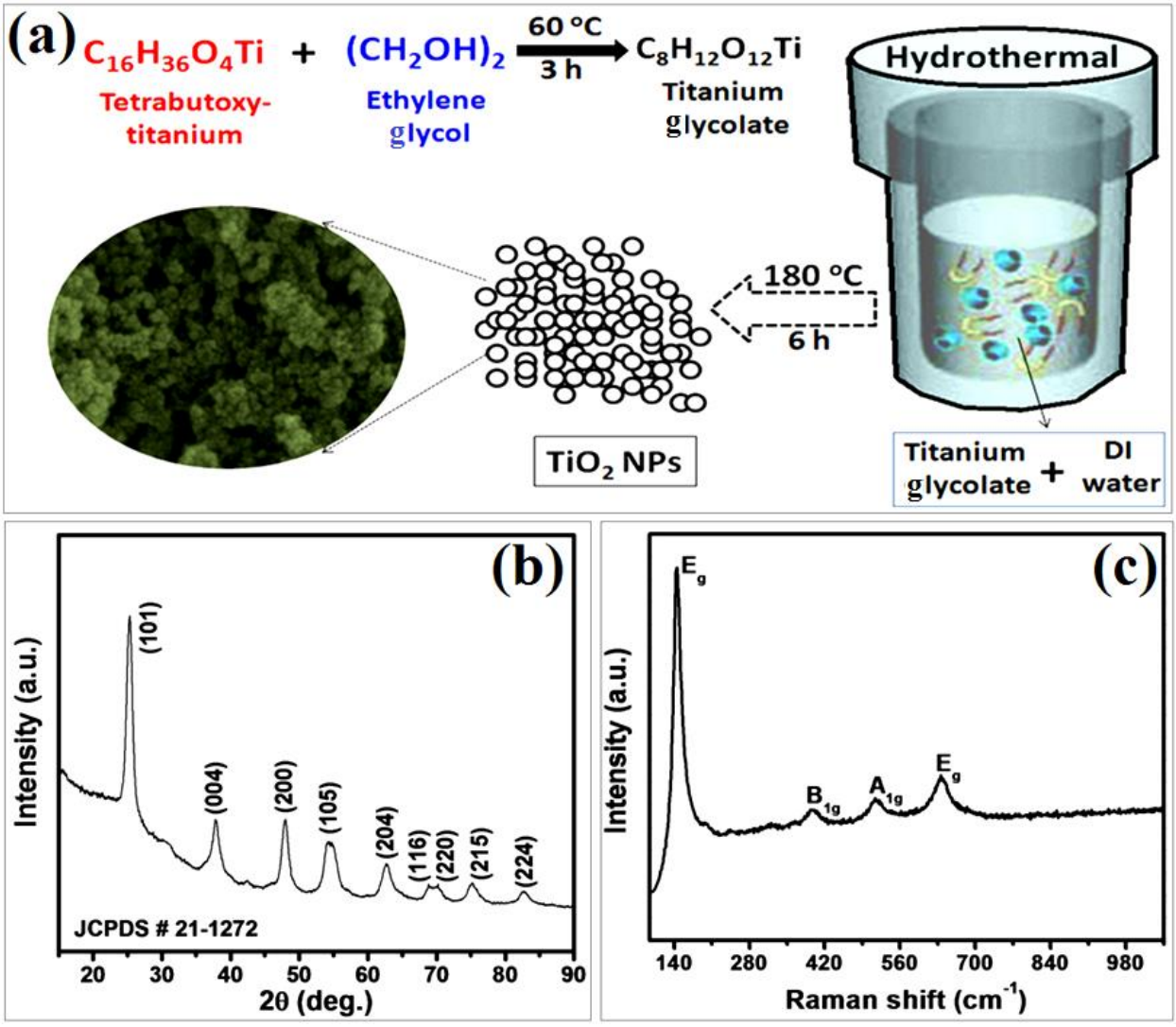

Fig. 1

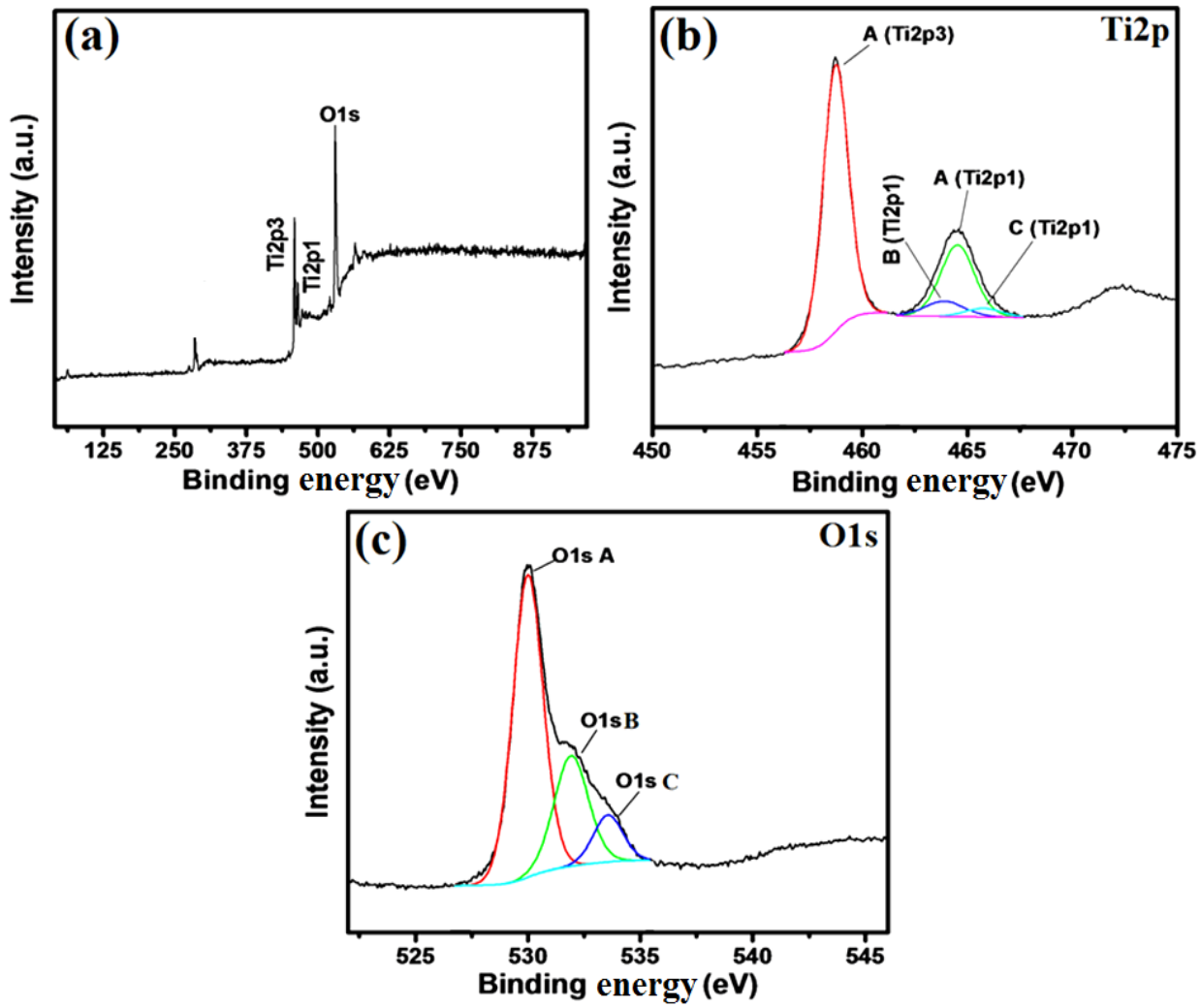

Fig. 2

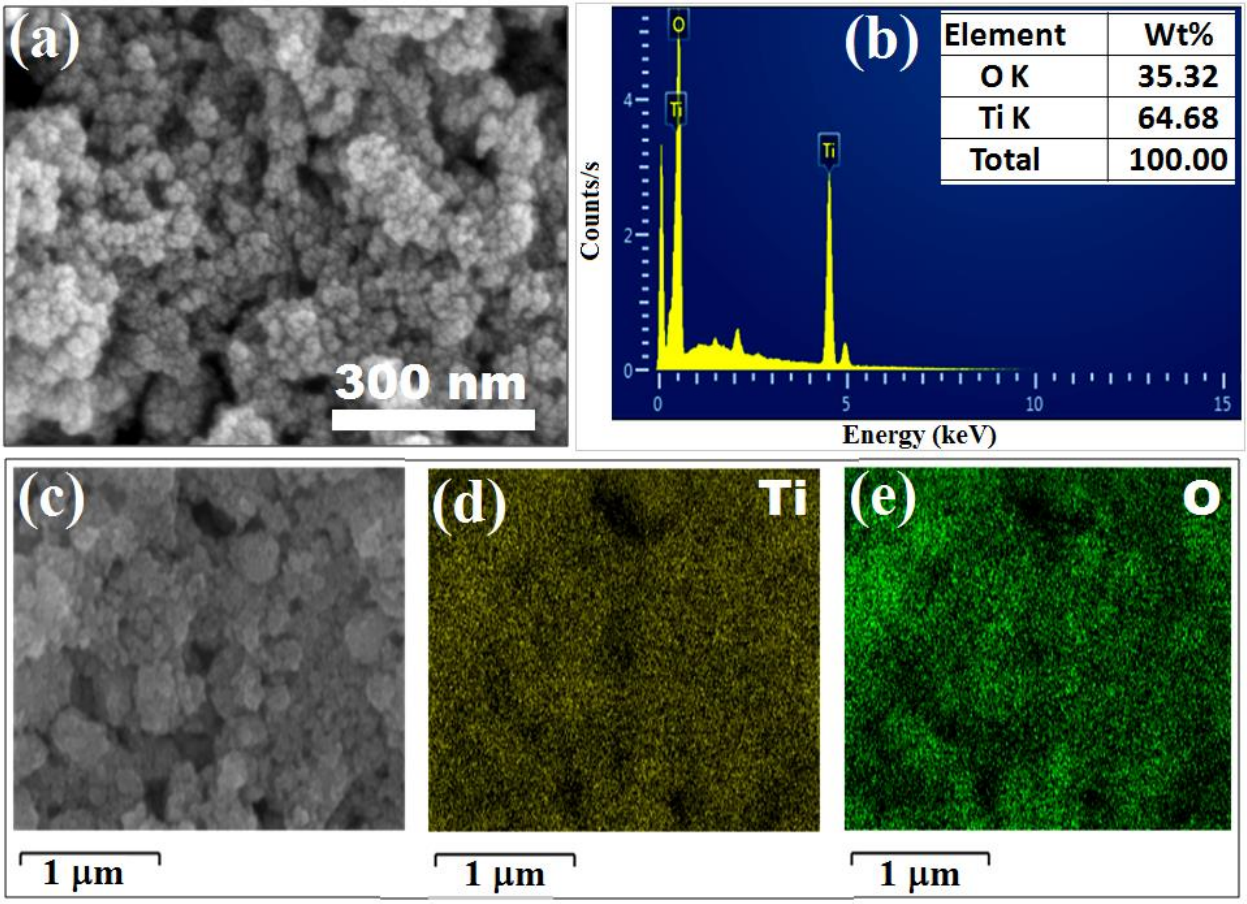

Fig. 3

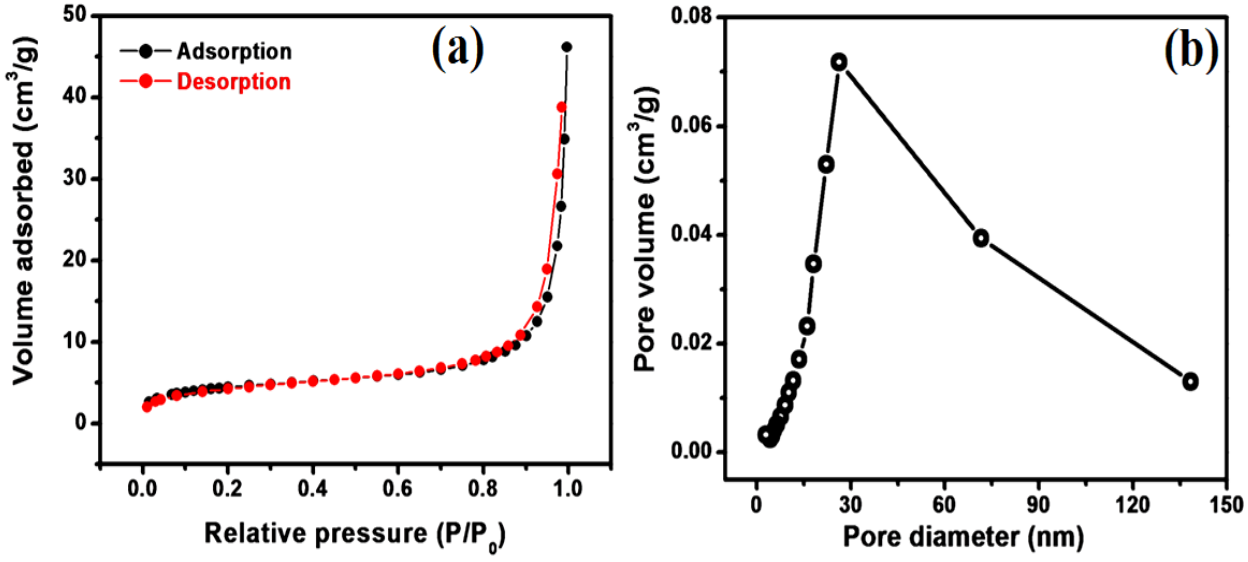

Fig. 4

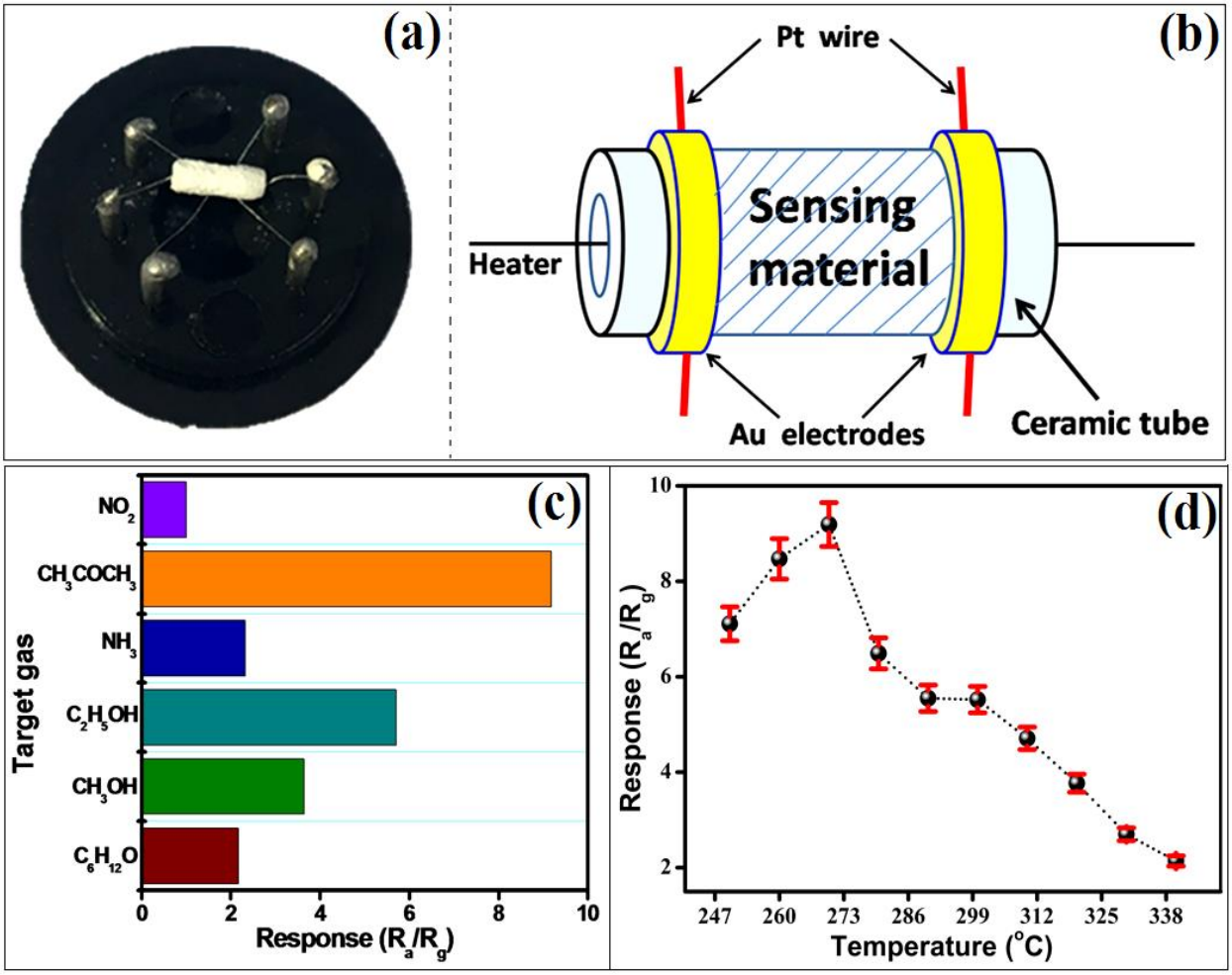

Fig. 5

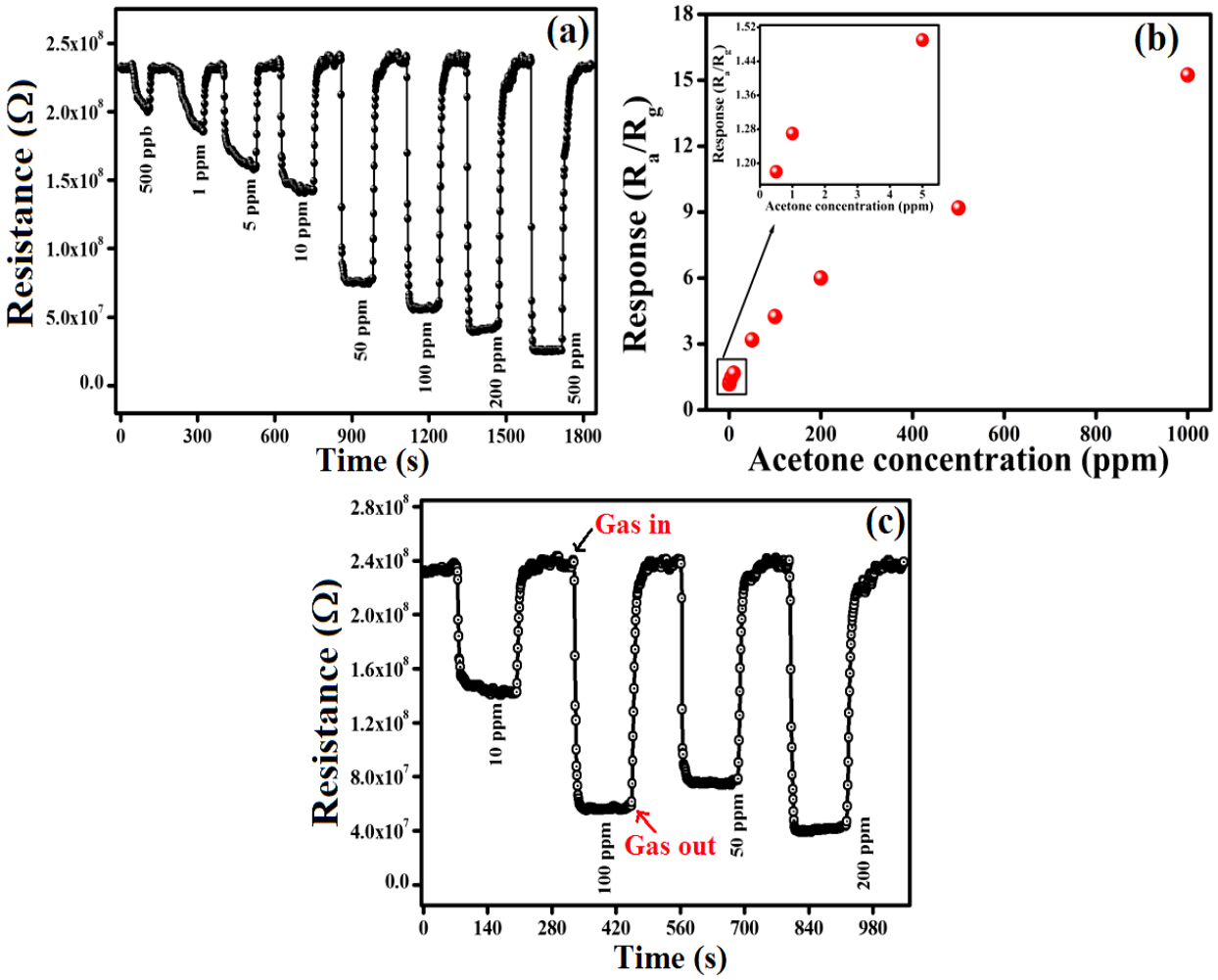

Fig. 6

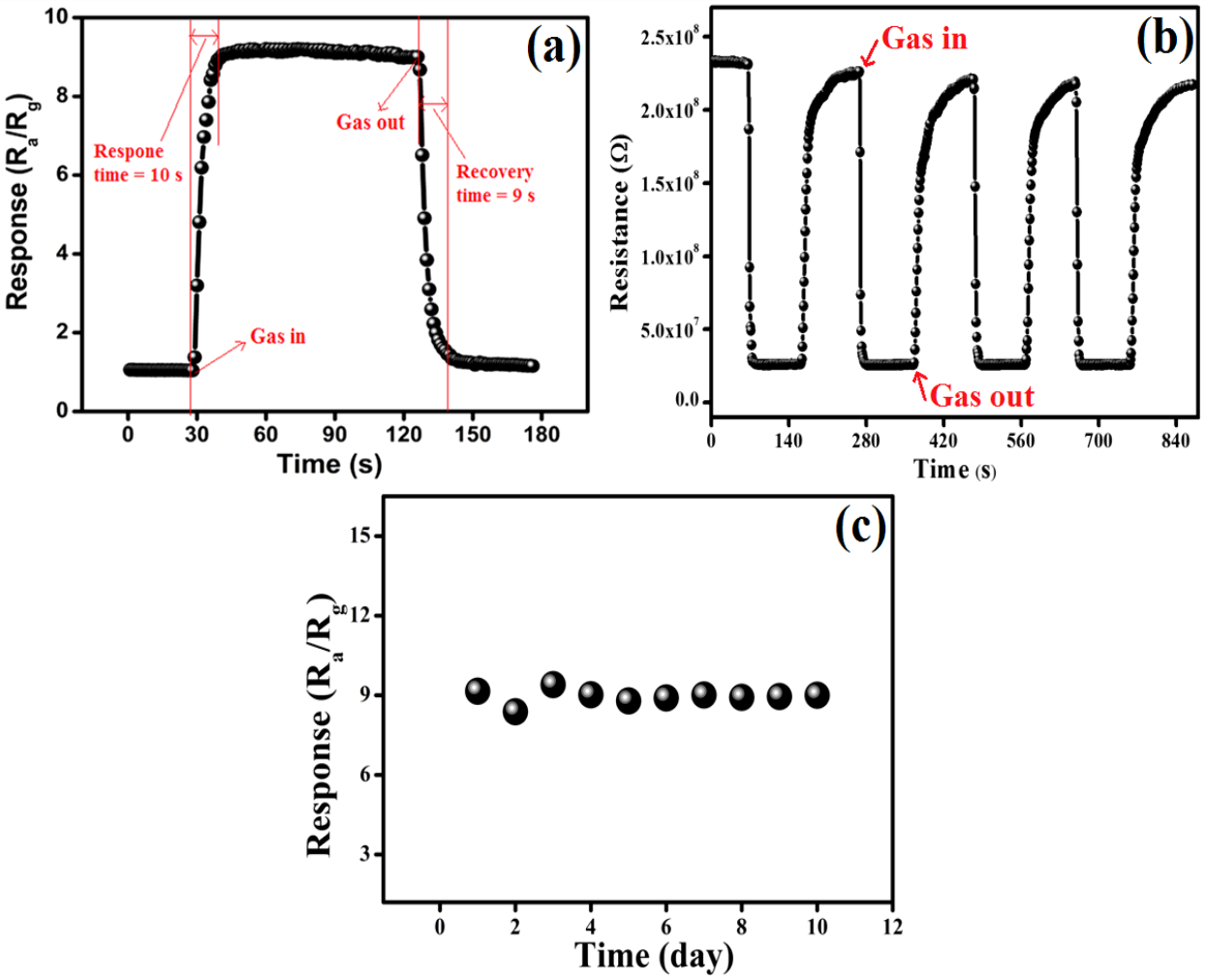

Fig. 7

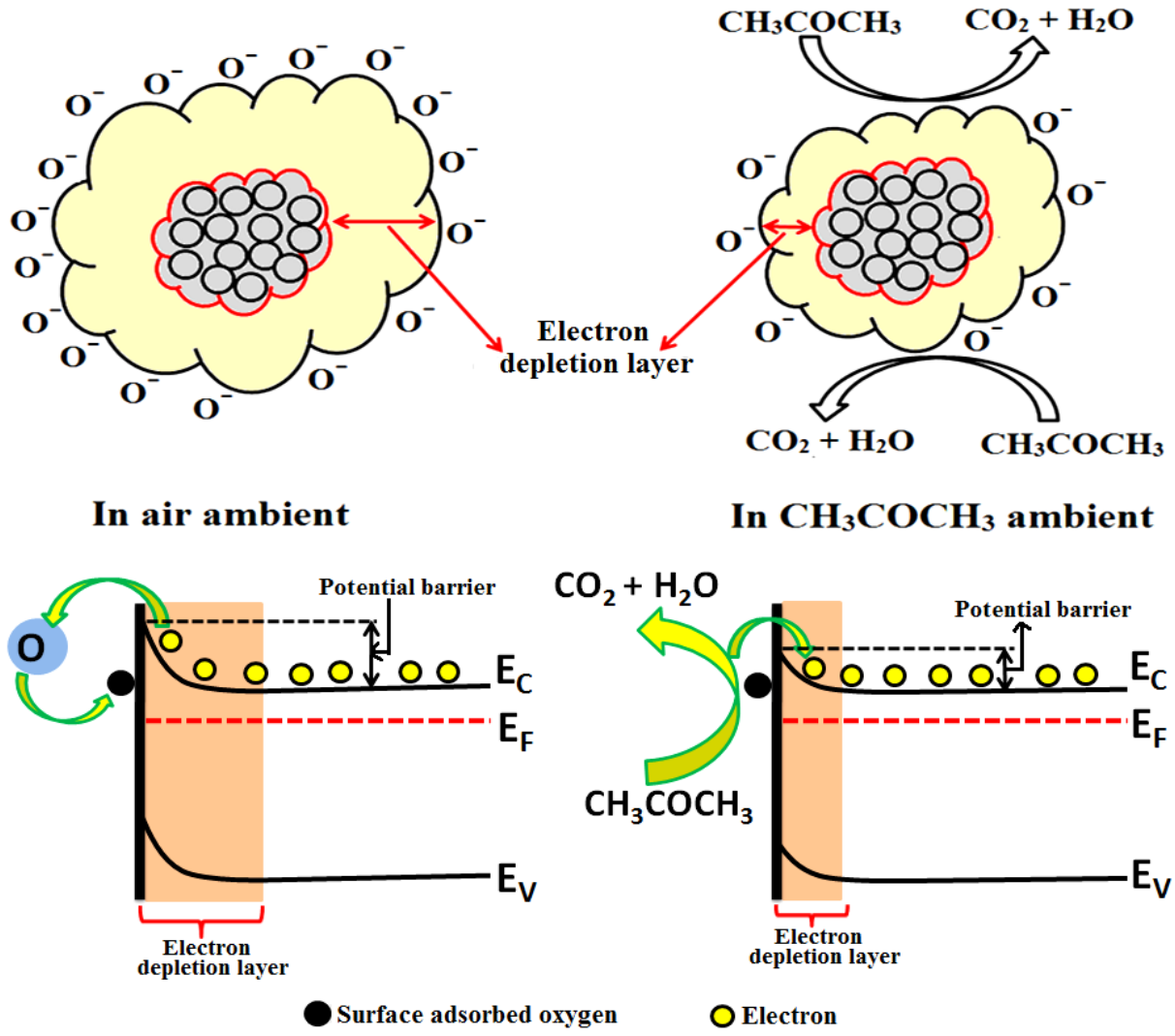

Fig. 8

Table 1: Comparison of gas sensing parameters of TiO_2 NPs sensor with other published CH_3COCH_3 sensors.

Table 1.

Material	Synthesis route	Sensor tempt.	Res (R_a/R_g)	Acetone (ppm)	Res-t	Rec-t	Lowest detection limit	Ref.
TiO_2 nanorods	Electrospinning	500 °C	~21	500 ppm	Several seconds	Several seconds	1 ppm	20
TiO_2NPs	Flame spray pyrolysis	400 °C	~6	400 ppm	Several min	Several min	25 ppm	21
TiO_2 hollow microspher-es	one-pot hydrothermal	320 °C	6.9	100 ppm	Several seconds	Several seconds	10 ppm	46
Ag-TiO_2NPs	Sol-gel	270 °C	8.9	1 ppm	29 s	2100 s	1 ppm	22
TiO_2 nanofl-owers	Hydrothermal route	60 °C	2.99	700 ppm	10 s	45 s	1 ppm	50
TiO_2 Nanotubes	Anodization	150 °C	2.9	500 ppm	100 s	180 s	10 ppm	23
Nanoporou-s TiO_2	Hydrothermal	370 °C	25.97	500 ppm	13 s	8 s	20 ppm	44
TiO_2NPs	Matrix assisted pulsed laser deposition	400 °C	6	100 ppm	240 s	-	20 ppm	24
Mesoporus TiO_2	Sol-gel	400 °C	53	400 ppm	-	-	100 ppm	47
TiO_2NPs	Screen printing	393 °C	1.51	1.5 ppm	50 s	50 s	1.5 ppm	25
TiO_2NPs	Matrix assisted pulsed laser deposition	350 °C	3.04	20 ppm	4 min	14 min	20 ppm	51
TiO_2 spherical collides	Sol-gel method	350 °C	2.3	1000 ppm	150 s	350 s	1000 ppm	52
TiO_2 NPs	**Hydrothermal**	**270 °C**	**9.19**	**500 ppm**	**10 s**	**9 s**	**500 ppb**	**This work**

Res = Response, Res-t = Response time, Rec-t = Recovery time.